Modelling the evolution of microstructural bands in a martensite/austenite Q&P-processed stainless steel

Li, Gaojie; Traka, Konstantina; Kwarkernaak, Kees; Gonzalez-Garcia, Yaiza; Santofimia, Maria J.

DOI
10.1016/j.scriptamat.2024.116457

Publication date
2025

Document Version
Final published version

Published in
Scripta Materialia

Scripta Materialia 257 (2025) 116457

Contents lists available at ScienceDirect

Scripta Materialia

journal homepage: www.journals.elsevier.com/scripta-materialia

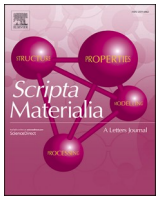

Modelling the evolution of microstructural bands in a martensite/austenite Q&P-processed stainless steel

Gaojie Li [1,*], Konstantina Traka [1,*], Kees Kwarkernaak, Yaiza Gonzalez-Garcia, Maria J. Santofimia

Department of Materials Science and Engineering, Delft University of Technology, Mekelweg 2, 2628 CD, Delft, the Netherlands

ARTICLE INFO

Keywords:
Q&P
Martensitic stainless steel
Phase transformation
Interface mobility
Cellular automata

ABSTRACT

This work discusses the microstructure evolution observed in a quenching and partitioning (Q&P)-processed martensite/austenite stainless steel during the partitioning step at 400 °C for 300 s, where distinct microstructural bands rich in austenite due to elemental segregation, evolve into a uniform distribution of austenite grains. This phenomenon is characterised and investigated using a model for the carbon partitioning from martensite to austenite coupled with the movement of the martensite-austenite interface. The observed elimination of microstructural bands is found to be related to the topological distribution of austenite grains and the heterogeneity of the thermodynamic equilibrium regime at the various interfaces governing the partitioning process. Furthermore, the concurrence of banding elimination (local equilibrium) and phase growth towards the global equilibrium phase fractions is investigated in the simulations in terms of the role of Mn. It is found that the local equilibrium-negligible partitioning (LENP) conditions lead to the most realistic outcome.

Quenching and Partitioning (Q&P) has been proposed [1–4] and developed over the last decades as a promising method to produce advanced high strength steels, including stainless steels, exhibiting good combination of strength and ductility. The Q&P treatment involves a quenching step in which a controlled fraction of austenite transforms into martensite. This step is followed by an isothermal heat treatment, known as partitioning step, in which carbon partitions from martensite and enriches the untransformed austenite [4,5]. Due to the high carbon enrichment of austenite, after the subsequent quenching the resulting microstructure preserves a controlled fraction of austenite, while the previously formed martensite is now carbon-depleted. The thermodynamics of the partitioning step are essential for the theoretical understanding of the process. Speer et al. [4] described the endpoint of carbon partitioning based on the so-called constrained carbon equilibrium (CCE) [6–8] conditions, which assume that the carbon partitioning from martensite to austenite ends when the chemical potential of carbon is equal in both phases. These assumptions are considered in the absence of carbide formation and interface mobility.

Building upon the work of Speer et al. [4], numerous research works have experimentally shown and theoretically demonstrated the possible interaction of the martensite/austenite interface movement with the process of carbon partitioning from martensite to austenite [9,10]. Particularly, the movement of the martensite-austenite interface during the partitioning step of the Q&P process has been detected in the literature through several different experimental techniques. For example, the interface motion has been revealed by simple observation of microstructures before and after partitioning with electron backscatter diffraction (EBSD) and through the application of in-situ heat treatments at the transmission electron microscope (TEM) [11,12]. The theoretical explanation of these interface phenomena, comes down to the chemical potential of the substitutional lattice being different between the two phases, thus leading to a driving force exerted at the phase boundaries. This mechanism leads to two different phenomena. The first and obvious expected process is the inevitable motion of the interface toward the global equilibrium phase fractions of martensite (body-centred cubic, BCC) and austenite (face-centred cubic, FCC). It should be clarified that global equilibrium is meant in the context of partitioning (i.e. no secondary phases, but phase equilibrium between BCC and FCC), specifically the regime at which iron and carbon in FCC are in equilibrium with iron, and carbon, respectively, in BCC, just as explained by Santofimia et al. [9]. The second process is the interface motion occurring based on the local and / or time-dependent carbon concentration at the

* Corresponding authors.
E-mail addresses: g.li-6@tudelft.nl (G. Li), C.Traka@tudelft.nl (K. Traka).
[1] These authors contributed equally to this work.

https://doi.org/10.1016/j.scriptamat.2024.116457
Received 31 May 2024; Received in revised form 25 October 2024; Accepted 7 November 2024
Available online 14 November 2024

interface. Since the interphases and the associated driving force only realize the local carbon concentrations, these would then depend also in the local topology. For example, we would expect that applying a modeling approach similar to [9] in a heterogeneous distribution of austenite, we would capture different behaviours regarding the phase growth due to the variations of carbon concentration at the different interfaces.

For this reason, the present work investigates the dynamics of martensite-austenite interfaces during the partitioning step of a Q&P-processed microstructure which exhibits topological heterogeneities in the austenite distribution. The aim is to investigate the local and temporal phase redistribution explained above, when carbon redistribution due to partitioning is heterogeneous, i.e. it takes place differently among the microstructure due to the different thermodynamic regimes. Specifically, we investigate a stainless steel that displays compositional segregation in the form of bands. It will be shown that the presence of microstructural bands in the form of austenite-rich and austenite-poor martensite/austenite locations after the first quench leads to a distinct evolution of phase fractions during the subsequent partitioning step that differs per location. Eventually, the microstructural banding is significantly reduced. This behaviour is modelled using a full field modelling approach of the concurring processes, i.e. carbon partitioning and interphase migration, showing that the main reason behind such a microstructural evolution is topological.

The material object of study is a hot-rolled and annealed stainless steel, the chemical composition of which is shown in Table 1. Cylindrical specimens with 10 mm in length and 4 mm in diameter were machined from the forged billet, and were heat-treated in a Bähr 805 DIL A/D dilatometer. A type S thermocouple spot-welded on the surface was used to monitor and control the temperature. Interrupted partitioning treatments were carried out to observe the changing microstructure. The specimens were first fully austenitised at 1100 °C for 15 min, and then quenched to room temperature. This experiment led to a martensite start temperature of 150 °C. Subsequently, the specimens were heated to 400 °C and held for 2 and 5 min, before being finally quenched to either room temperature or to −130 °C. The latter quench was done in order to measure the martensite start temperature associated to the austenite present in the microstructure after the partitioning steps. This led to 0 °C (for a 2-minute partition) and −45 °C (for a 5-minute partition), respectively. Due to the large uncertainty inherent to the determination of the Ms [13] temperature from the carbon concentration in austenite, here we used a procedure developed particularly for stainless steels [14]. The measurement of these martensite start temperatures has associated austenite with a carbon concentration of 0.28 ± 0.05 wt.% (quenched specimen), 0.57 ± 0.05 wt.% (2-minute partitioning) and 0.65 ± 0.05 wt.% (5-minute partitioning).

The microstructure of each specimen was investigated by a LEICA optical microscope. Specimens for microstructure characterisation were prepared by grinding from P800 to P2000 on abrasive papers and polishing with 3 μm and 1 μm diamond paste. Vilella etchant was used to reveal the microstructure by wiping it with a cotton swab from 10 s to 50 s. EBSD was performed using a Helios G4 PFIB, with an acceleration voltage of 20 kV and a working distance of 6 – 9 mm. Specimens for EBSD were mechanically ground and polished, including a final polishing step with OPS suspension for 20 min. Data acquisition was performed with a step size of 200 nm in areas of 200 μm x 200 μm. Post-processing was done using TSL OIM Analysis software, where martensite was characterised as BCC and austenite as FCC.

Phase fractions were quantified in the specimens by X-ray Diffraction (XRD) using a Bruker D8 Discover diffractometer equipped with an Eiger-2500k 2D-detector and Co Kα radiation. The diffractometer was operated with an acceleration voltage of 45 kV and a current of 35 mA. The scanning range of 2θ was 40° - 130° with a step size of 0.034° 2θ and a counting time of 2 s per step. The austenite volume fraction was calculated from the net integral intensities of the four austenite reflection peaks (111), (200), (220), and (311). The volume fraction of retained austenite in the different specimens was 0.28 ± 0.02 (quenched specimen), 0.26 ± 0.02 (2-minute partitioning) and 0.33 ± 0.02 (5-minute partitioning).

Table 1
Chemical composition of the investigated alloy (in wt%).

C	Mn	Si	Cr	Ni	Mo	V	Al
0.32	3.00	0.3	13.1	0.2	0.3	0.064	0.002

From the above-described results, the volume fraction of austenite in the alloy subjected to a 400 °C partitioning exhibits either a non-decreasing trend when the treatment lasts for 2 min or a slight increase when the partitioning is extended to a total of 5 min. The carbon content in the retained austenite increases as the partitioning time extends.

Fig. 1 shows the microstructure obtained after the first quenching (Fig. 1a), and after quenching and partitioning at 400 °C for 5 min (Fig. 1b). A structure formed by alternating bands can be clearly observed in both cases. Austenite, primary martensite and fresh martensite cannot be distinguished. Our previous work [14] revealed that the dark bands contain lower levels of Mn and Cr, whereas the light bands are rich in these elements. These variations in elemental content directly impact the local Ms temperature, most importantly due to the fact that Mn and Cr attract carbon, which changes even more drastically the Ms temperature prior to the first quenching. As a result, the Mn, Cr, C-rich bands exhibited lower Ms temperatures, leading to a higher fraction of austenite, while the Mn and Cr-poor bands exhibited higher Ms temperatures, suggesting a lower fraction of austenite. Fig. 2 displays the EBSD maps in scanned areas of 200 × 200 μm^2, perpendicular to the normal direction (ND) of the sheet. The top row shows austenite color-coded with inverse pole figure (IPF) along the ND and martensite is plotted as color-coded with image quality (IQ). The bottom row shows austenite color-coded with IPF along the ND and martensite is plotted as black. Though the scanned areas are, in any case, not sufficient to obtain reliable phase fraction quantifications, especially since the banding comes together with high heterogeneity in the statistics, it is noteworthy that the values obtained are quite consistent with the XRD measurements. Particularly, the fractions of retained austenite measured in the EBSD scans are 0.20 (quenched specimen), 0.28 (2-minute partitioning) and 0.31 (5-minute partitioning).

Note that the bands of austenite, as observed in the quenched specimen, are no longer present after partitioning for 2 min, suggesting a transformation or realignment of the microstructural features. After partitioning for 5 min, a consistent and uniform phase distribution is evident from the EBSD scans. The vast majority of retained austenite appears in the configuration of blocky shapes, positioned within the confines of prior austenite grains. Also, comparing the IQ in the various stages, it is evident that martensite has relaxed from carbon and/or strain, as the dark greyish pixels become lighter after annealing. Nevertheless, the absence of clear austenite bands does not imply a reduction in the compositional segregation since this is still noticeable by optical microscopy after partitioning for 5 min, as shown in Fig. 1b.

Particularly, the significant heterogeneity in austenite distribution observed in the microstructures after quenching is inherent to the carbon concentration variations between alloying-rich bands and alloying-poor bands. As indicated, the austenitic structure seems to evolve during the partitioning step into homogeneously distributed and similar in size austenite grains. Owing to low diffusivity of Mn and Cr, it is expected that under the present partitioning condition (400 °C for 5 min) only the redistribution of C plays a role in the microstructure evolution observed.

To understand the physical processes leading to these experimental findings, the microstructure development during the partitioning step is simulated using a model that couples carbon partitioning with phase redistribution. The model considers carbon redistribution due to interface partitioning [15] and mesoscale concentration gradients [16] as outlined in [17]. The interface migration is simulated based on the

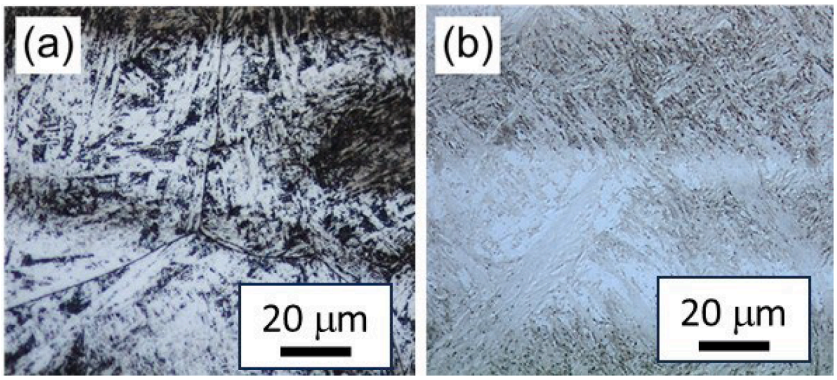

Fig. 1. Optical micrographs of specimens etched with Vilella agent (a) after quenching to room temperature and (b) after partitioning at 400 °C for 5 min.

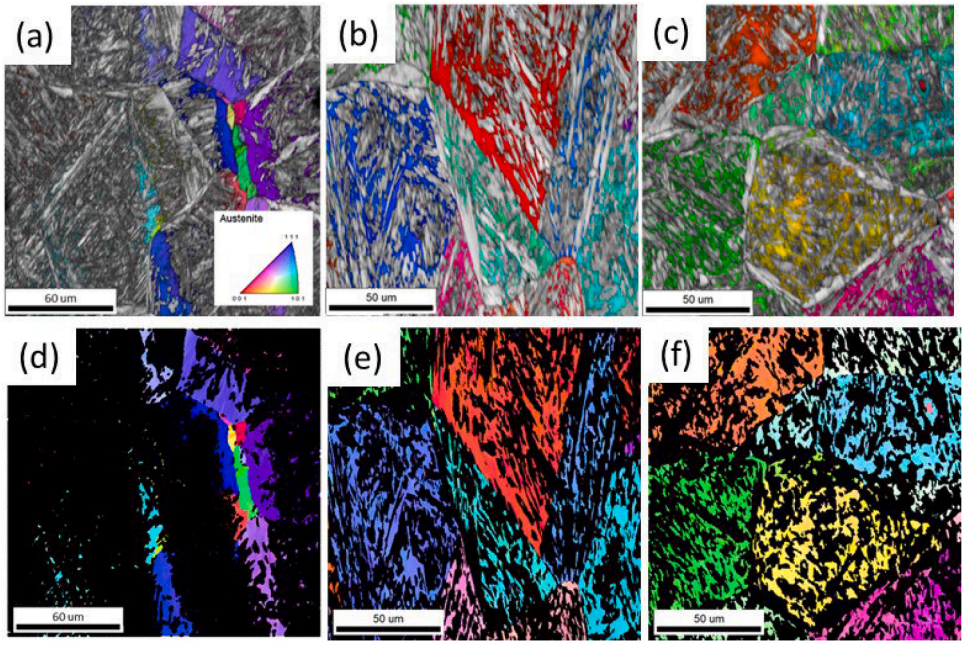

Fig. 2. EBSD maps at the three different quenching and partitioning stages investigated. The maps show the austenite crystal orientation colour-coded with inverse pole figure (IPF) along the normal direction (ND). Martensite is shown as colour-coded with image quality (IQ) in the top row and as black in the bottom row. (a and d) as-quenched, (b and e) after partitioning at 400 °C for 2 min, and (c and f) after partitioning at 400 °C for 5 min.

deterministic cellular automata approach [18] by using the short-range diffusion of the substitutional lattice description [19,20], driven by the local chemical potential difference, as explained in [9]. Carbide precipitation during partitioning, as proposed by Toji et al. [21] is not considered here because the aim of the study is to investigate whether the local topology is sufficient to explain the banding elimination. Although carbide formation may affect the banding elimination, it is not expected that it is exclusively responsible for it.

Regarding the modelling framework, the carbon redistribution occurs by the numerical description of concentration gradient-driven diffusion, with phase partitioning taking place as part of the numerical system, as explained in [17]. The local equilibrium of carbon at 400℃ is calculated for all possible local compositions, by setting equal the chemical potential of carbon in FCC and BCC, as calculated from Thermo-Calc using the TCFE13 database. The interface migration takes place based on the driving force arising from the chemical potential difference of iron between BCC and FCC for the given (simulated) local and temporal carbon concentrations. Also here, the chemical potentials were calculated using Thermo-Calc with the TCFE13 database.

The diffusivities of carbon in martensite and austenite used in the simulations, as well as the parameters associated with the mobility of the martensite-austenite interface, are displayed in Table 2. For a more detailed description of this model, as well as for its physical validation (i.e. grid sensitivity tests and global equilibrium) the reader is referred to the **Supplementary Material**. The model is implemented in OMicroN (optimising microstructures numerically) [17,19,22] and in CASIPT (cellular automata model for phase transformations) [17,19,23,24]. In all simulations performed in this work, the starting microstructure obtained by EBSD is imported into the model by a one-to-one fashion, i.e. every simulation cell assumes the crystal orientation and phase equal to

Table 2
Parameters used in the simulations.

Carbon diffusivity in martensite [$m^2\ s^{-1}$]	$1.06 \cdot 10^{-13}$	From Agren 1982, [28] at 400 °C.
Carbon diffusivity in austenite [$m^2\ s^{-1}$]	$6.1 \cdot 10^{-13}$	Effective for a carbon concentration of 3.8 wt.% (expected equilibrium) using Agren 1986 [29], at 400 °C.
Pre-exponential factor for interface mobility [mol m $J^{-1}\ s^{-1}$]	0.4	Based on theoretical arguments in [30–32] and investigations in [19,20].
Activation energy for interface mobility [kJ mol^{-1}]	140	Hillert 2006 [33].

the ones measured for the pixel in the same spatial coordinates. The 2D microstructures are resolved by square cells of grid spacing equal to 0.2 μm.

At first, we simulate carbon partitioning under the assumption of fixed interfaces, in order to demonstrate the associated local and temporal carbon concentration heterogeneity, as this will lead to heterogeneous interface migration. Notably, the simulation leads to some austenite sites being very highly enriched, reaching carbon concentration values (temporarily) that are even higher than 6.7 wt.% - an outcome that is common in partitioning simulations [25]. Specifically, although such high concentrations are unlikely to occur, since they only take place temporarily (i.e. before global equilibrium is reached), we do not transform such sites in cementite. Fig. 3 shows the spatial evolution of the carbon concentration under the assumption of immobile interfaces. A significant heterogeneity in the carbon concentration near the austenite/martensite interfaces is observed. In regions containing small austenite grains and/or fractions, such as the zoomed-in area on the left in Fig. 3, austenite becomes richer in carbon than in regions containing large austenite grains and/or fractions, e.g. the zoomed-in area on the right in Fig. 3. That is because the local fraction of austenite is significantly higher than the local fraction of martensite, and thus, carbon diffuses away from the interfaces to enrich the bulk austenite. The interphases surrounded by high carbon concentrations are expected to migrate toward martensite since austenite is thermodynamically more stable, and vice versa, martensite is expected to grow in the regions of low carbon concentrations. These phenomena are expected to take place, just as explained by Santofimia [9]. The heterogeneous motion of interfaces is inherent exclusively to the local and temporal carbon concentration distribution.

Fig. 4 shows the simulated microstructure where carbon partitioning is coupled with interface migration. Fig. 4a shows the simulated carbon distribution maps after partitioning at 400 °C for 0 s, 60 s, 120 s, and 300 s, whereas Fig. 4b displays the corresponding austenite distribution (crystal direction // ND). At the beginning of partitioning, the carbon concentration is homogeneously distributed, i.e. the concentration is everywhere equal to the alloy's carbon composition. After 60 s, carbon partitioning is evidenced by the higher carbon contents in small austenite phase particles (red areas in Fig. 4a) next to the martensite/austenite interfaces compared to those in the inner part (light blue area in Fig. 4a) of the austenite long blocks. As the partitioning time increases, the austenite grains gradually grow, and the inner part of the austenite blocks is replaced by martensite areas. After 300 s, the red-colored austenite grains are distributed uniformly across the matrix, thus revealing that the prior banded austenite structure is eventually almost replaced by uniformly distributed austenite grains of similar carbon concentration. The simulation results correspond well to the trends revealed by the EBSD observations and explain the phenomenon of the banding elimination.

Up to now, the simulations explain the banding elimination, but the global phase fractions are much lower than the experimentally obtained ones. Particularly, the simulated austenite fraction is 0.08, which aligns with the expected global equilibrium based on the Fe-C chemical potential equilibrium, whereas the experimental austenite fraction is 0.33. A possible reason is the role of martensite defects. It is known that, although in partitioning simulations martensite is treated as a phase identical to strained-free ferrite, in martensite-austenite microstructures the experimental phase fractions and the carbon concentrations are typically different from the equilibrium values [26]. Therefore, even in Fe-C materials, it is expected that the defects in martensite affect the partitioning evolution. Specifically, the carbon chemical potentials are affected and may lead to high localized carbon concentration in martensite, just as explained by Traka et al. [17]. Such a case would potentially result in localized austenite formation, as also observed in [12]. But also the iron chemical potentials, from the strain energy barrier in the martensite growth, as explained analytically by Behera and Olson [27]. Either way, i.e. due to local aspects or global equilibrium, the theoretical global equilibrium inherent to the present simulations is already expected not to reach the accurate austenite fractions.

Nevertheless, given the high manganese content of the present material, we take this opportunity to discuss an additional reason for the phase fraction evolution during partitioning, especially since we have two concurrent phenomena taking place, i.e. the banding elimination and the global phase fractions evolution. The banding elimination is not a result of the Mn content, but the evolution of global phase fractions is. Therefore, we can discuss the effects of Mn since now not only the bands should eliminate but also the austenite fractions should remain almost unchanged (i.e. like the experimental measurement). In the following, the effect of Mn on the interface migration during the carbon partitioning process is discussed. Particularly, the chemical potentials of carbon and substitutional lattice are considered in the simulations through three different systems and conditions at the martensite/austenite interface: iron-carbon, iron-carbon-manganese under para-equilibrium (PE) conditions and iron-carbon-manganese under local equilibrium-negligible partitioning (LENP) conditions. The LENP is incorporated by assuming that while the mesoscale Mn distribution is unaffected, the moving interfaces lead to the local partitioning of Mn in the austenite side of the austenite-martensite interface, i.e. every adjacent austenite-martensite cells have an average of 3.1 wt.% Mn during all simulated stages, whereas every interface separates infinitesimal areas of austenite with 6 wt.% Mn and martensite with 0 wt.% Mn. This means that the chemical potentials of carbon and substitutional lattice at the interface correspond to FCC with 6 wt.% Mn and BCC in the absence of Mn.

The corresponding simulation results are shown in Fig. 5 for the case

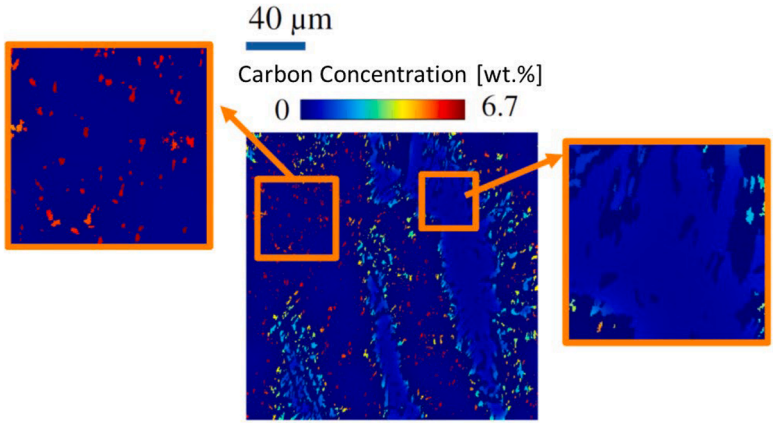

Fig. 3. Simulated carbon concentration during partitioning, under the assumption of fixed interfaces, in the system after partitioning at 400 °C for 300 s.

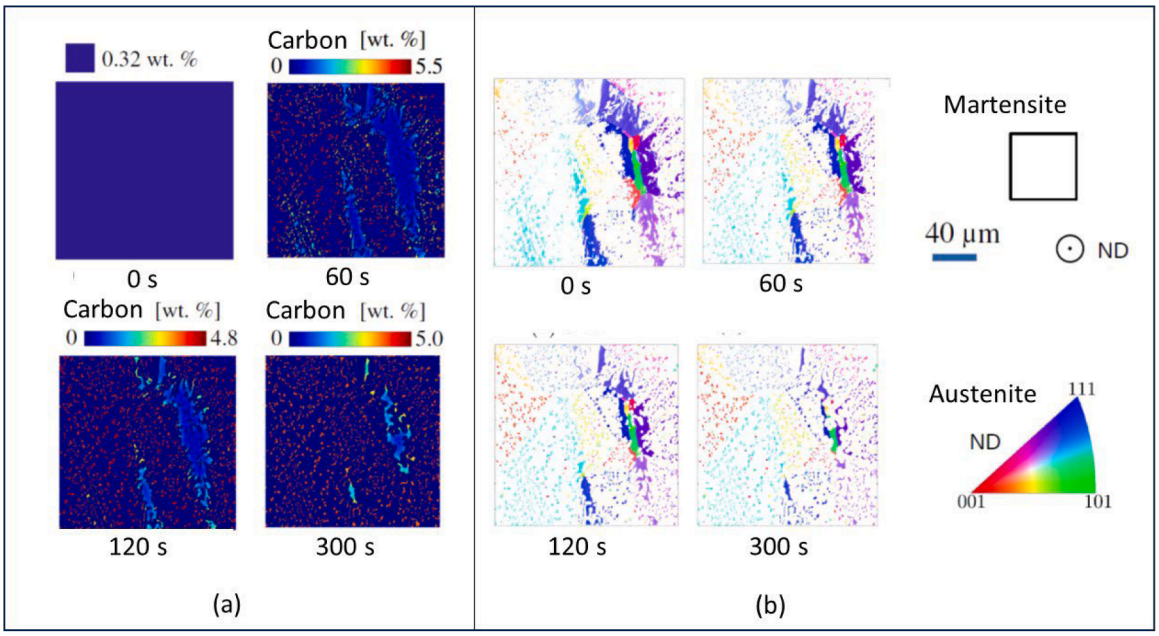

Fig. 4. Simulated evolution of the microstructure and carbon concentration in the system during partitioning at 400 °C assuming mobile martensite-austenite interfaces. (a) Carbon concentration and (b) crystal direction parallel to ND (inverse pole figure).

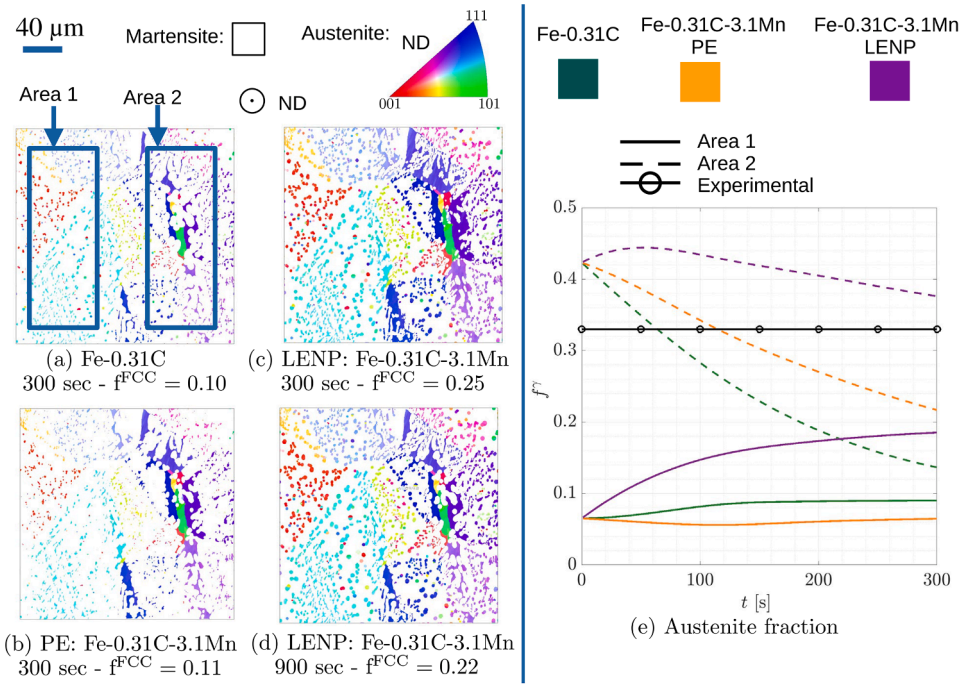

Fig. 5. Effect of Mn in the temporal microstructure evolution during partitioning, (a)-(d) show the outcome in the absence of Mn, including Mn and PE, and including Mn and LENP (300 s and 900 s), respectively. (e) shows the evolution of the austenite fraction in two different locations of the microstructure under the different conditions.

of partitioning at 400 °C. In order to understand the outcomes of this figure, it is important first to mention that the expected equilibrium fractions of austenite under the three different evaluated conditions are different, namely 0.09 for the Fe-C system, 0.11 for the Fe-C-Mn under PE and 0.20 for the Fe-C-Mn under LENP. This explains that after 300 s of partitioning at 400 °C, the simulations show that the fraction of austenite reached under the different conditions is 0.10 (Fe-C), 0.11 (Fe-C-Mn, PE) and 0.25 (Fe-C-Mn LENP), this last one evolving to a fraction of 0.22 after 900 s of partitioning at 400 °C. The close relation between the reached fraction of austenite and the expected from equilibrium under different conditions indicates that considering together the simulated band elimination and the austenite fraction evolution are indeed insightful to understand the role of Mn.

Particularly, the Fe-C case brings a fast elimination of the band, since martensite grows rapidly at the expense of the large austenite grains. However, the austenite phase fraction remains much lower than observed experimentally (0.31 in the EBSD scan of Fig. 2). Considering the effect of Mn under PE conditions leads to a slower elimination of the

bands, without any significant improvement in the prediction of the phase fractions. Altogether, it seems that the LENP conditions brings the most realistic outcome, where banding elimination, although slower, occurs, and at the same time the global fractions are closer to the experimentally observed. This becomes clearer in Fig. 5e, where the austenite fraction evolution is quantified in the two different areas indicated in Fig. 5a. Area 1 is initially austenite-poor and area 2 is initially austenite-rich. The only simulation where the austenite fraction evolution in both areas converges to the experimentally observed is the one performed under LENP conditions. In-situ investigations of the evolution of phase fraction and composition during the partitioning step in these materials may contribute to clarify the thermodynamic conditions governing the described processes.

To summarise, this work presents the evolution of a martensite-austenite microstructure of a stainless steel during the partitioning step of the Q&P process. Particularly, the influence of the microstructural heterogeneity inherent to the chemical composition distribution on the microstructure evolution and phase distribution is investigated. It is observed that the elemental segregation of Mn and Cr leads to a distribution of martensite start temperatures that leads to the presence of austenite bands at the quenching step. Although the elemental segregation bands persist during the partitioning step, there is a clear transition in the topological distribution of austenite, i.e. the microstructural bands have been eliminated and replaced by a relatively uniform (in phase distribution) microstructure. A partitioning model, considering carbon interphase partitioning, carbon diffusion, and interface migration, explained the evolution mechanism of banding elimination on the basis of the heterogeneity of the local carbon concentration and consequently driving force for interface migration. The simulations reveal that the heterogeneous phase distribution is sufficient to lead to heterogeneous partitioning regimes among the various interfaces, insofar as the banding ends up disappearing. In this work, we neglected carbide formation in order to isolate the possible causes of the observed banding elimination. Nevertheless, if carbides form heterogeneously, the induced chemical variations between different austenite grains would also lead to heterogeneous interface motions. A future investigation on the effects of chemical vs phase heterogeneity in the evolution of microstructural bands would be particularly insightful.

Finally, in view of the contradicting phenomena observed, i.e. the phase growth toward banding elimination and the phase growth toward global equilibrium, we took the opportunity to investigate different thermodynamic equilibrium assumptions. In terms of the role of Mn, the simulations showed that LENP conditions best described the observed microstructural evolution.

Data availability

The source files, executable, and input files are available open source in OMicroN (optimising microstructures numerically) https://github.com/k-traka/OMicroN [17,19,22].

CRediT authorship contribution statement

Gaojie Li: Writing – original draft, Investigation, Formal analysis, Data curation, Conceptualization. **Konstantina Traka:** Writing – original draft, Software, Investigation, Formal analysis, Conceptualization. **Kees Kwarkernaak:** Writing – review & editing. **Yaiza Gonzalez-Garcia:** Writing – review & editing, Supervision, Project administration, Funding acquisition. **Maria J. Santofimia:** Writing – review & editing, Supervision, Project administration, Funding acquisition, Conceptualization.

Declaration of competing interest

The authors declare that they have no known competing financial interests or personal relationships that could have appeared to influence the work reported in this paper.

Acknowledgements

This research has received funding from the European Union Research Fund for Coal and Steel (RFCS) under grant agreement N°847195, QPINOX project and from the European Union Research Fund for Coal and Steel (RFCS) under grant agreement N° 101034039, OPTIDAMATOL project.

Supplementary materials

Supplementary material associated with this article can be found, in the online version, at doi:10.1016/j.scriptamat.2024.116457.

References

[1] D.K. Matlock, J.G. Speer, Third generation of AHSS: microstructure design concepts, in: A. Haldar, S. Suwas, D. Bhattacharjee (Eds.), Microstructure and Texture in Steels, Springer London, London, 2009, pp. 185–205, https://doi.org/10.1007/978-1-84882-454-6_11. Eds.
[2] X. Hu, Z. Feng, Advanced high-strength steel - basics and applications in the automotive industry, ORNL/TM-2021/2047 (2021) 1813170, https://doi.org/10.2172/1813170.
[3] J.G. Speer, A.M. Streicher, D. Matlock, F. Rizzo, G. Krauss, Quenching and partitioning: a fundamentally new process to create high strength trip sheet microstructures, Materials Science and Technology 2003 Meeting (2003) 505–522.
[4] J. Speer, D.K. Matlock, B.C. De Cooman, J.G. Schroth, Carbon partitioning into austenite after martensite transformation, Acta. Mater 51 (9) (2003) 2611–2622, https://doi.org/10.1016/S1359-6454(03)00059-4.
[5] J.G. Speer, F.C.R. Assunção, D.K. Matlock, D.V. Edmonds, The 'quenching and partitioning' process: background and recent progress, Mat. Res. 8 (4) (2005) 417–423, https://doi.org/10.1590/S1516-14392005000400010.
[6] M. Hillert, J. Ågren, On the definitions of paraequilibrium and orthoequilibrium, Scr. Mater. 50 (5) (2004) 697–699, https://doi.org/10.1016/j.scriptamat.2003.11.020.
[7] J.G. Speer, D.K. Matlock, B.C. DeCooman, J.G. Schroth, Comments on 'On the definitions of paraequilibrium and orthoequilibrium' by M. Hillert and J. Ågren, Scripta Materialia, 50, 697–9 (2004), Scr. Mater. 52 (1) (2005) 83–85, https://doi.org/10.1016/j.scriptamat.2004.08.029.
[8] M. Hillert, J. Ågren, Reply to comments on 'On the definition of paraequilibrium and orthoequilibrium, Scr. Mater. 52 (1) (2005) 87–88, https://doi.org/10.1016/j.scriptamat.2004.08.026.
[9] M.J. Santofimia, L. Zhao, J. Sietsma, Model for the interaction between interface migration and carbon diffusion during annealing of martensite–austenite microstructures in steels, Scr. Mater. 59 (2) (2008) 159–162, https://doi.org/10.1016/j.scriptamat.2008.02.045.
[10] M.J. Santofimia, J.G. Speer, A.J. Clarke, L. Zhao, J. Sietsma, Influence of interface mobility on the evolution of austenite–martensite grain assemblies during annealing, Acta Mater 57 (15) (2009) 4548–4557, https://doi.org/10.1016/j.actamat.2009.06.024.
[11] S. Dieck, P. Rosemann, A. Kromm, T. Halle, Reversed austenite for enhancing ductility of martensitic stainless steel, IOP Conf. Series: Mater. Sci. Eng. 181 (2017) 012034, https://doi.org/10.1088/1757-899X/181/1/012034.
[12] L. Yuan, D. Ponge, J. Wittig, P. Choi, J.A. Jiménez, D. Raabe, Nanoscale austenite reversion through partitioning, segregation and kinetic freezing: example of a ductile 2GPa Fe-Cr-C steel, Acta Mater 60 (6–7) (2012) 2790–2804, https://doi.org/10.1016/j.actamat.2012.01.045.
[13] H.S. Yang, H.K.D.H. Bhadeshia, Uncertainties in dilatometric determination of martensite start temperature, Mater. Sci. Technol. 23 (5) (2007) 556–560, https://doi.org/10.1179/174328407X176857.
[14] G. Li, C. Kwakernaak, A. Smith, M. Muratori, Y. Gonzalez-Garcia, M.J. Santofimia, Microstructure development of quenching and partitioning-processed martensitic stainless steels with different manganese content, Mater. Sci. Technol. 40 (6) (2024) 449–465, https://doi.org/10.1177/02670836231215989.
[15] S. Matas, R.F. Hehemann, Retained austenite and the tempering of martensite, Nature 187 (4738) (1960) 685–686, https://doi.org/10.1038/187685a0.
[16] A. Fick, Ueber diffusion, Ann. Phys. Chem. 170 (1) (1855) 59–86, https://doi.org/10.1002/andp.18551700105.
[17] K. Traka, J. Sietsma, M.J. Santofimia, Modeling the interaction of carbon segregation to defects and carbon partitioning in multiphase steels, Acta Mater 277 (2024) 120204, https://doi.org/10.1016/j.actamat.2024.120204.
[18] J.G. Kemeny, Theory of self-reproducing automata. John von Neumann. Edited by Arthur W. Burks. University of Illinois Press, Urbana, 1966. 408 pp., illus. $10, Science 157 (3785) (1967) 180, https://doi.org/10.1126/science.157.3785.180.–180.
[19] K. Traka, K. Sedighiani, C. Bos, J.G. López, K. Angenendt, D. Raabe, J. Sietsma, Topological aspects responsible for recrystallization evolution in an IF-steel sheet – Investigation with cellular-automaton simulations, Comput. Mater. Sci. 198 (2021) 110643, https://doi.org/10.1016/j.commatsci.2021.110643.

[20] K. Traka, Investigations of the Early Stages of Recrystallization in Interstitial-Free and Low-Carbon Steel sheets, Ph.D. Thesis, Delft University of Technology, (2022). do i: 10.4233/UUID:962F6655-A1B8-4C38-8467-0B2B651AB629.
[21] Y. Toji, G. Miyamoto, D. Raabe, Carbon partitioning during quenching and partitioning heat treatment accompanied by carbide precipitation, Acta Mater 86 (2015) 137–147, https://doi.org/10.1016/j.actamat.2014.11.049.
[22] K. Traka, E. Sepulveda-Hernandez, T. Nguyen-Minh, K. Sedighiani, J. Sietsma, L.A. I. Kestens, Prediction of different recrystallisation textures under a single unified physics-based model description, Comput. Mater. Sci. 246 (2025) 113425, https://doi.org/10.1016/j.commatsci.2024.113425.
[23] C. Bos, M.G. Mecozzi, J. Sietsma, A microstructure model for recrystallisation and phase transformation during the dual-phase steel annealing cycle, Comput. Mater. Sci. 48 (3) (2010) 692–699, https://doi.org/10.1016/j.commatsci.2010.03.010.
[24] C. Bos, M.G. Mecozzi, D.N. Hanlon, M.P. Aarnts, J. Sietsma, Application of a three-dimensional microstructure evolution model to identify key process settings for the production of dual-phase steels, Metall. Mater. Trans. A 42 (12) (2011) 3602–3610, https://doi.org/10.1007/s11661-011-0696-x.
[25] A.S. Nishikawa, M.J. Santofimia, J. Sietsma, H. Goldenstein, Influence of bainite reaction on the kinetics of carbon redistribution during the Quenching and Partitioning process, Acta Mater 142 (2018) 142–151, https://doi.org/10.1016/j.actamat.2017.09.048.
[26] S. Kumar, Quenching and partitioning (Q&P) process: a critical review of the competing reactions, Mater. Sci. Technol. 38 (11) (2022) 663–675, https://doi.org/10.1080/02670836.2022.2062646.
[27] A.K. Behera, G.B. Olson, Nonequilibrium thermodynamic modeling of carbon partitioning in quench and partition (Q&P) steel, Scr. Mater. 147 (2018) 6–10, https://doi.org/10.1016/j.scriptamat.2017.12.027.
[28] J. Agren, Diffusion in phases with several components and sublattices, J. Phys. Chem. Solids 43 (5) (1982) 421–430, https://doi.org/10.1016/0022-3697(82)90152-4.
[29] J. Agren, A revised expression for the diffusivity of carbon in binary Fe-C austenite, Scr. Metall. 20 (11) (1986) 1507–1510, https://doi.org/10.1016/0036-9748(86)90384-4.
[30] C.S. Smith, Grains, phases, and interphases: an interpretation of microstructure, *Trans. Metall. Soc.* AIME 175 (1948) 15–51.
[31] C.S. Smith, Grain shapes and other metallurgical applications of topology, Metallogr. Microstruct. Anal. 4 (6) (2015) 543–567, https://doi.org/10.1007/s13632-015-0241-1.
[32] J.E. Burke, D. Turnbull, Recrystallization and grain growth, Progress in Metal Physics 3 (1952) 220–292, https://doi.org/10.1016/0502-8205(52)90009-9.
[33] M. Hillert, L. Hoglund, Mobility of α/γ phase interfaces in Fe alloys, Scr. Mater. 54 (7) (2006) 1259–1263, https://doi.org/10.1016/j.scriptamat.2005.12.023.